Journal of Materials Chemistry B

ROYAL SOCIETY OF CHEMISTRY

COMMUNICATION

View Article Online
View Journal | View Issue

Cite this: J. Mater. Chem. B, 2024, 12, 9695

Received 6th March 2024,
Accepted 28th July 2024

DOI: 10.1039/d4tb00482e

rsc.li/materials-b

A natural multifunction and multiscale hierarchical matrix as a drug-eluting scaffold for biomedical applications†

Gabriela Graziani, ‡§*[a] Carla Triunfo,§[b] Giulia Magnabosco, ¶§[b] Simona Fermani,[bc] Devis Montroni, [b] Daniele Ghezzi,[d] Martina Cappelletti,[d] Nicola Baldini*[ae] and Giuseppe Falini *[b]

Sea urchin spines are biogenic single crystals of magnesium calcite that are stiff, strong, damage tolerant and light and have a bicontinuous porous structure. Here, we showed that the removal of their intraskeletal organic matrix materials did not affect the compressive mechanical properties and generated an open porosity. This matrix was able to adsorb and release oxytetracycline, a broad-spectrum antibiotic. The drug-loaded sea urchin matrix induced bacterial cell death after 4 and 8 hours of incubation of both Gram-negative *E. coli* and Gram-positive *S. aureus* strains and this process induces an inhibition of bacterial cell adhesion. In conclusion, this study shows that thermally treated sea urchin spines are a compressive resistant and lightweight matrix able to load drugs and with potential use in spine fusion, a challenging application that requires withstanding high compressive loading.

Introduction

Sea urchins have been populating Earth's oceans for over 450 million years,[1] adapting to challenging environments. During their evolution they have developed a wide variety of spine types, which serve as a defense mechanism against predators.[2] These spines need to be stiff, strong, damage-tolerant, and lightweight in order to fulfil their biological function.[3]

In contrast to mammals, which rely on hydroxyapatite, all the skeletal components of sea urchins are composed of Mg-calcite $(Ca_{1-x}Mg_x)CO_3$, which is grown and regenerated by the complex processes of biomineralization.[4] Elemental analysis has shown that the Mg distribution in single spines is not uniform: the Mg content increases from the tip to the base by an average of about 2 mol%.[5] This structural inhomogeneity occurs through the segregation of Mg-rich particles, which creates compressive stresses on the host matrix and improves mechanical properties.[6,7] As a consequence, the mechanical properties of the spine are also graded along this gradient.

Phyllacanthus imperialis (Lamarck 1816) is a species of sea urchins in the family Cidaridae widely distributed throughout the Indo-Pacific region and commercially available. The primary spines of this species vary in size from the oral side, where they are comparatively short, to the aboral side where they can be more than 10 cm long. These latter protect the echinoid from predators and serve as locomotion as well as mechanical fixation structures between the reefs.[1]

Under uniaxial compression the spines of *P. imperialis* possess a high crushing strength, σ_c, of 60 ± 10 MPa.[8] The energy-consuming breaking of these structures follows a layer-by-layer crushing mode, which keeps the lower layers of the material intact.[9] This is caused by the hierarchic structure of the spine, which extends from the microscale down to the nanoscale.

As generally observed in sea urchin spines in *P. imperialis* also the spine is arranged in three main structural areas from the outer to the inner structure: cortex, and stereome, which is articulated in a radiating layer and a medulla (the spine core).[8,10] The stereome has a complex bicontinuous porous structure,[11,12] which exhibits controlled gradients in porosity, reaching up to 75 vol%.[13] This porosity also changes in the different region of the stereome, showing an average pore diameter of 20.2 μm in the radiating layer and 18.6 μm in the

[a] Biomedical Science, Technologies, and Nanobiotecnology Lab, IRCCS Istituto Ortopedico Rizzoli, Bologna, Italy. E-mail: gabriela.graziani@polimi.it, nicola.baldini@ior.it
[b] Department of Chemistry "Giacomo Ciamician", University of Bologna, Bologna, Italy. E-mail: giuseppe.falini@unibo.it
[c] Interdepartmental Centre for Industrial Research Health Sciences & Technologies, University of Bologna, 40064 Bologna, Italy
[d] Department of Pharmacy and Biotechnology, University of Bologna, Bologna, Italy
[e] University of Bologna, Department of Biomedical and Neuromotor Sciences, Bologna, Italy

† Electronic supplementary information (ESI) available. See DOI: https://doi.org/10.1039/d4tb00482e

‡ Department of Chemistry, Materials and Chemical Engineering "G. Natta", Politecnico di Milano, Milan, Italy.
§ These authors equally contributed.
¶ Institute of Particle Technology, Friedrich-Alexander-University Erlangen-Nürnberg, Erlangen, Germany.

medulla, respectively, with an average strut thickness of 17.8 μm and 18.6 μm.[14]

The hierarchical open-cell structure of sea urchin spines is similar to that of human trabecular bone and possesses suitable mechanical properties for shaping. Therefore, they have been studied for potential applications in bone defect repair.[15] Indeed, Mg-substituted tricalcium phosphate (β-TCMP) scaffolds were produced by hydrothermal conversion of sea urchin spines.[8,16,17] This material drastically decreased its mechanical performance with respect to the pristine material, but, when implanted in rabbit femoral defects and degraded, it was replaced by newly formed bone.[17]

In this work we assume that the mechanical performances of the sea urchin spine are mainly related to geometrical factors and can be preserved after a thermal treatment that slightly modifies its composition.[11,18] Moreover, we expect that the thermal treatment, which removes the intra-crystalline organic matrix and water, can generate an additional apparent porosity.[19] Here, these two envisioned features are combined to fabricate a novel drug delivery platform. In particular, we show that antibiotics can be effectively loaded in the sea urchin-based scaffolds, and that the drug can be released and exert its antibacterial action. We select an antibiotic since, to date, orthopedic prostheses are always soaked in antibiotics prior to being implanted in the patient, so the route we propose here can be an alternative to the current gold standard practice. As a future perspective, the approach can be translated to the release of other drugs, for instance antimicrobial compounds (*i.e.* essential oils), which do not promote bacterial resistance or antitumoral drugs, since the spine is also the main site for bone metastases. This study represents a preliminary study for the manufacturing of the future scaffold for hard tissue regeneration based on sea urchin spines. In particular, it targets long-term release of antibiotics for application in spine fusion, a challenging *etc.* that requires withstanding high compressive loading and is burdened by a high infection rate and possible failure. Different from traditional delivery systems based on particles at different sizes, as mesoporous silicon nanoparticles,[20,21] for spine fusion the scaffold is expected to remain in the implantation site for 6/12 months,[22] and be progressively dissolved by bone cells (osteoclasts) and converted into mature bone.

Results and discussion

Aboral adult spines from *P. imperialis* with an average length of 70 mm (Fig. 1A) were used in this study. The samples were cut from the central region of the spine forming cylindrical shapes with a length of 5 mm and a diameter of approximately 8 mm (Fig. 1B). This aspect ratio was chosen to prevent bending and buckling during the uniaxial compression tests.[23] By selecting the central region along the length of the spine, we ensured compositional and structural homogeneity between samples. Previous studies have shown that both the stereom architecture (including the relative content of medulla, radiating layer, and cortex) and the Mg content change along the spine's main axis.[5,24]

Thermal treatment at 250 °C for various durations significantly removed the organic matrix and intra-skeletal water, which appeared to be completed after 8 hours. Longer thermal treatments, *i.e.* 24 and 48 hours, did not result in a significant increase in material loss due to heat (Table 1). The temperature choice was based on previous studies investigating changes in crystallographic parameters following thermal treatment.[25] Additionally, it was taken into consideration that higher temperatures can negatively impact mechanical properties.[26] For this reason, even if in other studies higher temperatures were used to completely remove intraskeletal materials, we decided to work with a lower temperature. This still ensure a completion of the pyrolytic process after the 8 hours of thermal treatment, as demonstrated for other biominerals.[19] This heating process also caused the colored pigments to be lost or degraded, resulting in the spine becoming whitish (Fig. 1C). This removal enhanced the material's biocompatibility as only the mineral phase remained, with no organic molecules from organism biosynthesis being present.[27] This removal is an important step for future biomedical applications, since non-human proteins may induce an immunologic response in the patient.

The removal of the intra-skeletal material also resulted in an increment in apparent nano-porosity. Indeed, the specific surface area increased from about 3 $m^2\ g^{-1}$ to about 5 $m^2\ g^{-1}$ (see Table 1), which aligns with previous studies.[19,28] Other studies have also reported an increase in specific surface area when biogenic calcium carbonate is thermally treated.[19,29] Additionally, we observed an increase in the overall porosity of the samples after the thermal and bleaching treatment, as shown in Fig. 2. It is worth noting that specific surface area and porosity did not increase when the thermal treatment exceeded 8 hours.

The observation by using SEM of the cross section of the spine revealed additional information (Fig. 3). The macroscopic

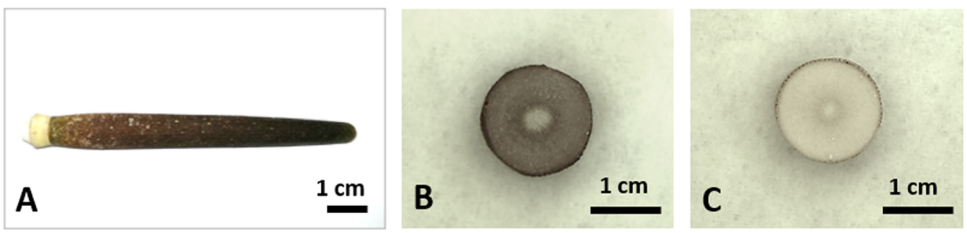

Fig. 1 Aboral adult spine from *P. imperialis* (A), 5 mm high disk before (B) and after the thermal treatment at 250 °C for 8 hours (C).

Table 1 Compositional and macro-textural data from samples of *P. imperialis* spines that were thermally treated at 250 °C for 0 hours (A, untreated), 8 hours (B), 24 hours (C) and 48 hours (D). The weight loss between 150 and 475 °C was used to estimate the content of intra-skeletal material (OM), the porosity (ϕ) was determined gravimetrically, and the surface area was measured using the BET method. At least 5 independent specimens were measured for each sample set

Sample	Time (hours)	OM[a] (wt%)	Porosity (ϕ) (%)	Surface area ($m^2\ g^{-1}$)
A	0	2.0 ± 0.5	50 ± 2	3.4 ± 0.5
B	8	0.9 ± 0.2	58.1 ± 0.4	4.7 ± 0.4
C	24	1.08 ± 0.05	58.6 ± 0.4	5.1 ± 0.6
D	48	0.85 ± 0.07	58 ± 1	5.0 ± 0.5

[a] The ANOVA test showed that the intraskeletal content of the pristine spines decreased significantly after the thermal treatment ($p < 0.001$).

structural organization of the spine remained unaltered by the thermal treatment, as expected.

In the selected region of the spine, the cortex showed a compact structure, while the radiating layer and medulla had an open structure. The radiating layer occupied the majority of the volume. As we moved from the medulla to the radiating layer, the average diameter of the struts decreased from 10 ± 3 μm to 7 ± 2 μm. The pore size was higher in the medulla (20 ± 4 μm) compared to the radiating layer (15 ± 3 μm). These data are slightly different from those reported by Grossmann and Nebelsick,[24] who analysed the entire spine along the longitudinal section. This may suggest an elongated morphology of pores for this species.

The cross-section also revealed conchoidal fractures in the struts, which occurred in both the medulla and the radiating layer (Fig. 4). This unique cleavage was observed in both the pristine and thermally treated samples. Since this effect did not appear to be related to the presence of the organic matrix, which was removed in the thermally treated samples, we can attribute it to geometric factors and the specific orientation of the crystallites in the sea urchin spine.[7,11,18]

The distribution of Mg in the sea urchin spine section was also evaluated by energy dispersive spectroscopy (EDS). The data show that the content of Mg was lower in the medulla (5.3 mol% $MgCO_3$) than in the radiating layer (8.1 mol% $MgCO_3$), with the lowest content in the cortex (5.0 mol% $MgCO_3$) (Fig. S1, ESI†). These data agree with the measurements reported in the literature.[30]

Diffractometric analyses showed that the mineral phase, Mg-calcite, did not change upon the thermal treatments (Fig. S2, ESI†). However, we found that the removal of the intraskeletal materials, such as water and organic matrix, provoked a slight change in lattice parameters, as already discovered by Pokroy's research team.[25,31,32] The *a*-axis and *c*-axis expanded by about 0.07% and 0.1%, respectively (Table S1, ESI†). A decrease in the content of ACC was also observed, from about 8 wt% to 5 wt%. These observations are consistent with those reported for *Paracentrotus lividus* spines after a thermal treatment.[33]

Under bulk compression all studied sea urchin spines, both pristine and thermally treated exhibited similar qualitative fracture behaviour, which was characterized by graceful failure. An image showing characteristic fractured materials and a representative load distance curve is reported in Fig. 5.

In the first phase of the load–distance curve, the specimens showed the formation of cracks limited to the external surface of the samples. This caused the external part of the specimen to separate into lath-like segments, which then spalled as the crosshead continued to move (Fig. 5A–C). Once the external section was completely crushed, the next inner part exhibited the same features. Axial cracks continued to form and damaged segments spalled until the spine was completely destroyed. Fig. 5D shows an example of the load-distance diagram for *P. imperialis* specimens, where the load of the sample was directly measured from the crosshead motion of the machine. Initially, an increase in load resulted in an elastic response until the force suddenly and significantly decreased due to crack formation and spalling. This process was limited to the inner part and did not extend further. Subsequently, there was a repeated slow increase in load followed by a sudden drop. The entire spine absorbed energy by crushing and segmenting under compression, preventing complete catastrophic failure. The compression strength and Young's modulus of the samples are reported in Table S2 (ESI†). They show that there were no relevant differences between pristine and thermally treated samples. However, the samples treated for 48 hours had the lowest values of compression strength and Young's modulus. A similar behavior in mechanical performance was observed for *Heterocentrotus mamillatus* spines after thermal treatment.[34]

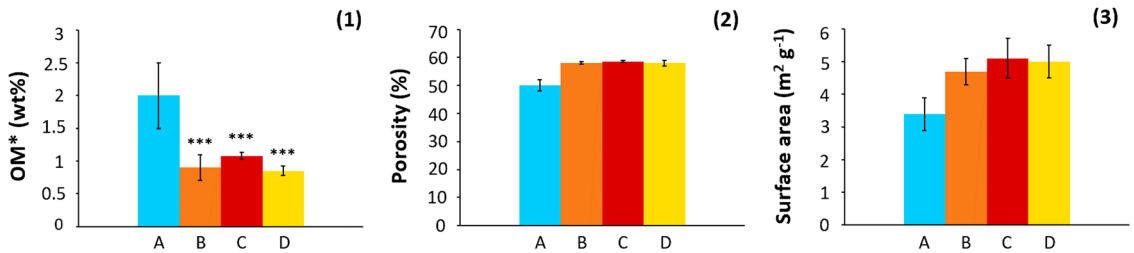

Fig. 2 Compositional and macro-textural data from samples of *P. imperialis* spines that were thermally treated at 250 °C for 0 hours ((A), untreated), 8 hours (B), 24 hours (C) and 48 hours (D). (1) The weight loss between 150 and 475 °C was used to estimate the content of intra-skeletal material (OM); (2) the porosity was determined gravimetrically; (3) surface area was measured using the BET method. At least 5 independent specimens were measured for each sample set. * The ANOVA test showed that the intraskeletal content of the pristine spines decreased significantly after the thermal treatment (***$p < 0.001$).

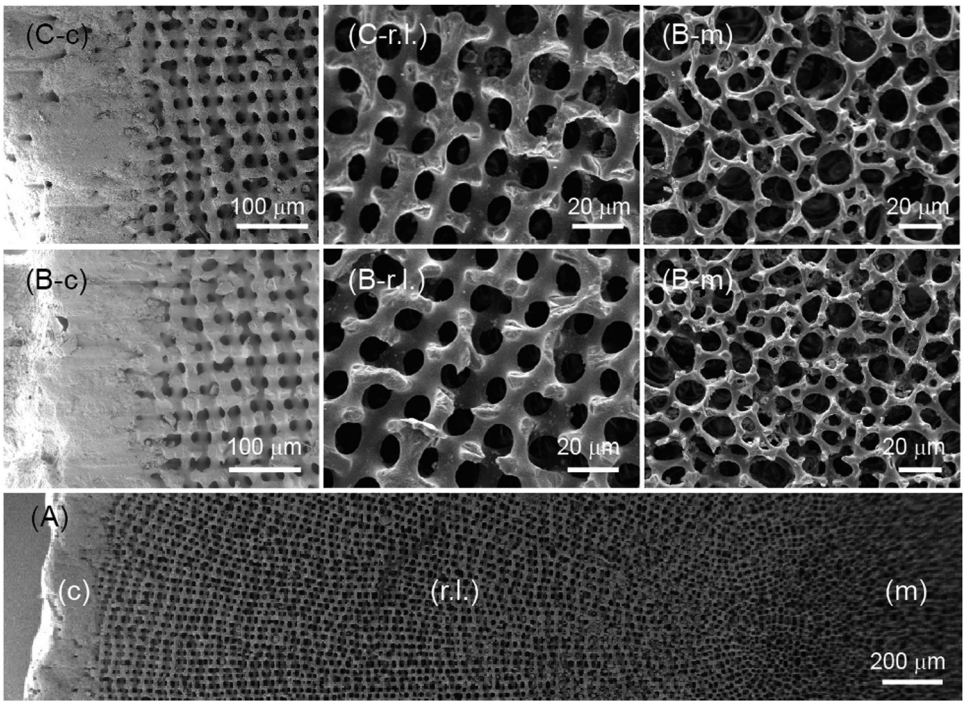

Fig. 3 Scanning electron microscopy images showing a cross-section of a sea urchin spine. (A) The ultrastructural organization of the *P. imperialis* spine presents three different regions: the central medulla (m), the intermediate radiating layer (r.l.), and the external cortex (c). (B) and (C) images show high magnifications of the three regions of the spine. The images labeled with (B) are untreated, while those labeled with (C) underwent 8 hours of thermal treatment. These images are representative of all investigated samples.

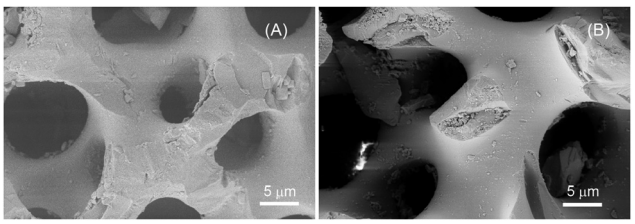

Fig. 4 SEM images of broken struts in the radiating layer of untreated (A) and 8 hours thermally treated (B) sea urchin spines.

This peculiar mechanical behaviour can be explained by considering the beneficial interconnectivity between the pore walls, which improves the resistance of the material under compression.[19,20,34] This interconnectivity appears promising for application in spinal cord implants, where catastrophic rupture must be avoided to prevent damage to the spinal cord.

The *P. imperialis* spines treated at 250 °C for 8 hours were used as substrates for the adsorption of the broad-spectrum antibiotic, oxytetracycline. Only the 8-hour treated ones were tested since they showed significantly similar properties to the other sample sets but with the shortest treatment time. The results indicated that the substrates reached adsorption saturation in 2 mL of a 15 μM solution within 24 hours, with a mean maximum adsorption capacity of 0.026 ± 0.004 mg g^{-1}. The desorption process was investigated in PBS and showed that the release reached a maximum after approximately 1 hour. Subsequently, there was an apparent re-sorption of the drug (Fig. S3, ESI†). Photodegradation of the drug was ruled out as the adsorption spectrum did not change after adsorption on the substrate (Fig. S4, ESI†). The desorption curve did not fit a Langmuir profile, suggesting that both chemical and physical adsorption processes were involved. Moreover, it should be noted that in PBS, a mineral transition from calcium carbonate to calcium phosphate can occur on the surface of the matrix.[35,36]

After demonstrating the capability of the *P. imperialis* spines to absorb and release drugs, we investigated their ability to inhibit bacterial growth. The data from the bacterial cell growth experiments (Fig. 6A and B) indicated that the spines loaded with oxytetracycline cause a gradual death of bacterial cells after 4- and 8-hour incubation of both Gram-negative *Escherichia coli* and Gram-positive *Staphylococcus aureus* strains. In both cases, there was an ~3 log reduction (equivalent to a 99.9% CFUs reduction) at the latest time point. This suggested that the release profile was suitable for the intended application and that the loaded oxytetracycline exhibits strong antibacterial activity regardless of the main bacterial cell envelope structures (which are associated with the classification of bacteria as Gram-negative or Gram-positive). Furthermore, the antibacterial activity of the antibiotic added directly to the medium at the same concentration used to load the sea urchin spines showed a similar trend over time (Fig. S5A and B, ESI†), indicating that the oxytetracycline loaded onto the sea urchin spines was almost completely released in the medium.

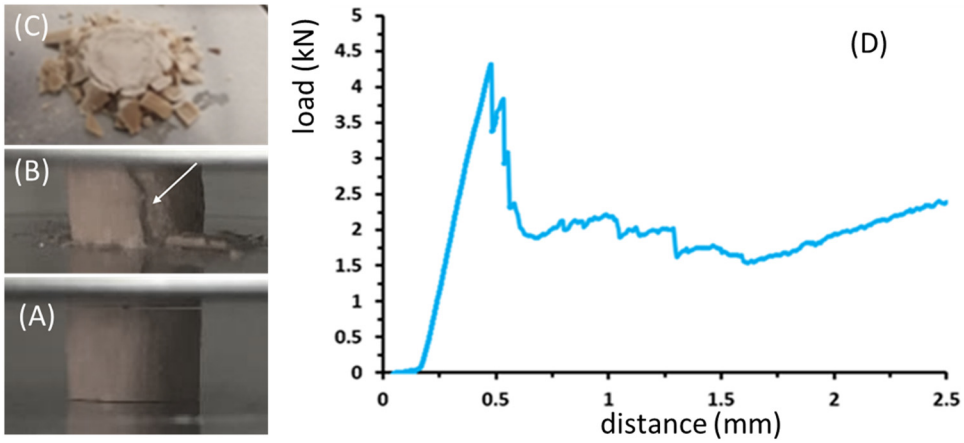

Fig. 5 *P. imperialis* disk fracture phases (A)–(C) and a typical experimental load-distance curve for the mechanical properties of the specimen (D). Side view of the sample under compression when (A) the sample is compressed in its elastic region and (B) it starts to have a crack on the external surface (see the white arrow). (C) shows a top view of the sample after compression.

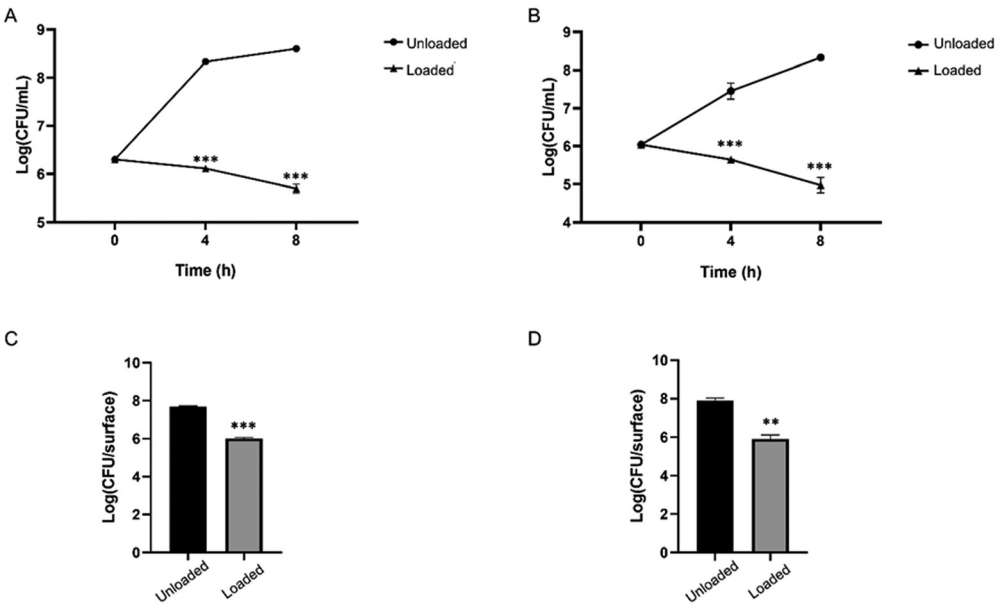

Fig. 6 Antibacterial and anti-adhesion activities of the loaded sample from *P. imperialis* towards *Escherichia coli* ATCC 8739 (panels (A) and (C)) and *Staphylococcus aureus* ATCC 6538P (panels (B) and (D)). Significance is indicated as follows: $^{**}p < 0.01$ and $^{***}p < 0.001$. Unloaded *P. imperialis* specimens were used as control.

We also examined the ability of the loaded samples to inhibit bacterial cell adhesion, which is one of the initial steps in bacterial biofilm formation. Our results show a significant anti-adhesion activity against both *E. coli* and *S. aureus* (Fig. 6C and D), with a reduction of 1.68 and 1.99 log (equivalent to a 97.92% and 98.96% reduction in CFUs), respectively, compared to the unloaded sample. Also in this case, the anti-adhesion activity on the (unloaded) sea urchin spines immersed in the culture medium added with oxytetracycline was similar against both bacterial strains (Fig. S5C and D, ESI†).

Previous studies reported the antimicrobial potential of sea urchin through organic solvent extracts of bioactive molecules from diverse body parts, including the spine.[37,38] In our case, the sea urchin spine (without antibiotic loading) did not show any antibacterial activity. This indicates that the antimicrobial activities observed in our experimental conditions are solely attributed to the loaded antibiotics. This is likely due to the removal of organic matrix protein molecules through the thermal treatment.

Conclusions

This study marks for the first time the use of thermally treated sea urchin spines as a carrier matrix. The matrix has been

found to have increased porosity and is devoid of biological macromolecules. It is able to withstand compression, is lightweight, and has the capability to load and release drugs.

Although further studies will need to be performed to investigate *in vitro* and *in vivo* biocompatibility of the substitutes, as well as their capability to promote bone regeneration and, hence, fusion, we foresee a potential application of this matrix in spine fusion, a challenging process that demands the ability to endure high compressive loads.

Materials and methods

Reagents and solvents were purchased from Merck and used without any further purification. Fresh solutions were prepared daily for each experiment. A skeleton of *P. imperialis* was purchased from Mostra Mondiale Malacologia in Cupra Marittima, Italy.

For substrate preparation, sea urchin spines measuring 6 cm to 8 cm in length and 5 mm to 10 mm in diameter were manually detached from the skeleton. They were then cut into 5 mm high disks using a precision diamond wheel saw. The disks were first cleaned with tap water and mechanically stirred in pure ethanol for 2 hours. Different treatments were applied to the samples to remove the organic matrix from the surface and increase its microporosity. Initially, the disks were soaked in the solution and gently stirred, setting them on a rocking table in a 5 vol% sodium hypochlorite solution for 24 hours. Then, they were stirred in a 1 M NaOH solution for 1 hour, washed with deionized water, and air dried. Finally, the disks were thermally treated in a muffle at 250 °C for 8, 24, and 48 hours to test different heating times.

Porosity

The porosity of the spine segments and spine cylinders was determined gravimetrically by assuming a density of 2.711 g cm^{-3} for Mg-calcite. Therefore, the volume of the spine segments and cylinders was calculated by measuring the area of the cross-section, A, on optical microscopy images using ImageJ, and multiplying it by the mean height, h. Together with the mass, m, the porosity was estimated using the following equation:

$$\phi\ (\%) = (1 - (m[g]/(A[cm^2] \times h[cm] \times 2.711[g \times cm^{-3}]))) \times 100$$

Thermal analysis

Thermogravimetric analysis (TGA) was performed using an SDT Q600 V 8.0 instrument (TA Instruments). The system was pre-equilibrated at 30 °C, then a ramp from 30 to 600 °C with a heating rate of 10 °C min^{-1} was performed under a nitrogen flow (100 mL min^{-1}). The measurement was performed on 10 mg of material on six independent specimens for each sample set. The temperature range considered to estimate the content of intraskeletal organic matrix was between 150 °C and 475 °C. The analysis of variance (ANOVA) was performed using the software SPSS 12.0 to compare the mean organic matrix content after different heating times.

Scanning electron microscopy observation

The morphological structure of the sea urchin spine disk surface was observed using a ZEISS Leo 1530 Gemini field emission scanning electron microscope (SEM) operated at 5 kV. The disks were dried under vacuum in a desiccator and 10 nm gold-coated before observation. EDS spectra and maps were collected on samples without any coating using a ZEISS Evo LS10 under low pressure operating at 30 kV using an X-ray EDS spectrometer Bruker Quantax 200 × 30 mm^2. Brunauer–Emmett–Teller measurements: the BET specific surface area was measured on an ASAP 2020 micromeritics instrument using N_2 as an absorbent at liquid N_2 temperature (77 K). Before measurements, the samples were degassed at 403.15 K for 24 hours. Each sample set was measured on XX g of the material on X independent specimens.

X-Ray powder diffraction analyses

X-ray powder diffraction (XRPD) measurements were performed using a PanAnalytical X'Pert Pro diffractometer equipped with an X'Celerator detector with Cu Kα radiation in the range 20–60° 2θ, step size 0.02° 2θ, and counting time 180 s per step. The evaluation of the ACC was carried out using about 20 wt% of diamond as an internal standard. All the structural and compositional parameters were refined using the Profex software.

Compression tests

The mechanical properties of the sea urchin spine disks were evaluated through compression tests using an Instron universal testing machine (Illinois Tool Works Inc., Norwood – MA, United States of America) equipped with a 5 kN load cell. The load was applied using a 5 cm diameter compression platen moved at a constant downward speed of 0.5 mm min^{-1}. The measurement was performed at least six specimens for each sample set.

Adult aboral spines of *P. imperialis* were used as samples for the mechanical characterization. Several aboral spines were sectioned perpendicular to the *c*-axis with a diamond saw (Buehler med 1000, ITW Test and Measurement GmbH, Esslingen, Germany) using a blade thickness of 1 mm. In this way, spine segments were fabricated with coplanar ends for the uniaxial compression tests. The coplanar ends are required to achieve uniform loading during the uniaxial compression experiments. The samples tested had a cylindrical shape with a diameter of around 5.5 mm and a height of 5 mm.

The compression strength, σ_c, was calculated from the load at the first crack formation. Young's modulus, E, was calculated from the slope of the linear elastic increase in the stress (σ)–strain (ε) plots.

Oxytetracycline adsorption and desorption test

The *P. imperialis* cylinders were first treated with a 5 vol% sodium hypochlorite solution for 24 hours to remove all

possible organic contaminants from the surface, then washed with deionized water and air dried. Adsorption kinetics experiments were carried out by immersing a 5 mm high cylinder from the *P. imperialis* spine in 2 mL of a 15 μM oxytetracycline aqueous solution at pH 8.7. This concentration is well below the toxicity threshold of the antibiotic, that is identified in the literature to be above 40 μM.[39]. The samples were kept in a 20 mL glass tubes at room temperature under mechanical stirring. To evaluate the drug absorption a spectrum of the solution was recorded at 0, 24, and 48 hours after the loading. The experiment was performed six times, and for each trial, the drug solution was transferred into a plastic cuvette with a 1 cm optical path. The oxytetracycline desorption test was performed at room temperature (about 25 °C) by immersing each drug-loaded *P. imperialis* cylinder in 2 ml of PBS in a vial placed on a rocking table to shake. The concentration of the drug desorbed in solution was calculated *via* absorbance measurements after 10 min, 30 min, 1 hour, 2 hours, 4 hours, 6 hours, 8 hours, 24 hours, and 48 hours. The antibiotic concentration in solution was measured at 370 nm using a UV-vis spectrophotometer (Cary 300 Bio, Agilent Technologies) with a spectral range of 200–800 nm.

Microbiological tests

The antibacterial activity of the oxytetracycline-loaded samples was evaluated by analyzing the inhibition of the growth of the two reference pathogenic bacterial strains *Escherichia coli* ATCC 8739 and *Staphylococcus aureus* ATCC 6538P. All cultures were prepared by inoculating a single bacterial colony (pre-grown on Luria-Bertani (LB) agar (1.5% agar w/v) plates for 18–20 hours) in 50 mL tubes with 5 mL of LB liquid medium. Cultures were grown overnight at 37 °C under agitation and then diluted to reach a final concentration of around 10^6 CFU mL^{-1}. For the test, the control (samples without oxytetracycline) and the loaded samples were placed at the bottom of 48-well microplates. Each well was then inoculated with 500 μL of the bacterial suspension, and the microtiter plate was incubated for 8 hours at 37 °C under shaking conditions (130 rpm). The growth of the bacteria was assessed after 4 and 8 hours of incubation by spreading serial dilutions of cultures on LB agar plates and counting the number of CFU mL^{-1} after 18–24 hours of static incubation at 37 °C. Triplicates were performed for each experimental condition. The same procedure was performed to test the antibacterial activity of the oxytetracycline added into the culture medium at the concentration used to load the sea urchin spines against the growth of both bacterial strains.

To test the anti-adhesion activity, the bacterial suspensions of *E. coli* ATCC 8739 and *S. aureus* ATCC 6538P grown overnight were diluted to reach 10^8 CFU mL^{-1}. The control (samples without absorbed oxytetracycline) and the loaded samples were placed at the bottom of 48-well microplates that were filled with 500 μL bacterial suspension and further incubated for 4 hours at 37 °C under gentle shaking conditions (50 rpm). The samples were removed from the cultures, gently washed in saline solution (NaCl 0.85 w/v%) to remove the non-adherent cells, placed in 2 mL tubes filled with 1 mL of saline solution, and sonicated for 5 min to detach the adherent cells. The number of adherent cells was finally assessed by spreading serial dilutions of cultures on LB agar plates and counting the number of CFU $surface^{-1}$ after 18–24 hours of static incubation at 37 °C. Triplicates were performed for each experimental condition. The same procedure was performed to test the anti-adhesion activity (on unloaded sea urchin spines) of the oxytetracycline added into the culture medium at the same concentration used to load the sea urchin spines.

Data availability

Raw data will be made available under request to the corresponding author.

Conflicts of interest

There are no conflicts to declare.

Acknowledgements

This work was supported by funding from the National Recovery and 674 Resilience Plan (PNRR), Mission 4 Component 2 Investment call for tender no. 3138 of 16 December 2021, rectified by Decree no. 3175 of 18 December 2021 of Italian Ministry of University and Research funded by the European Union NextGenerationEU, project code CN_00000033, Concession Decree no. 1034 of 17 June 2022 adopted by the Italian Ministry of University and Research, Project title ''National Biodiversity Future Center-BFC''. N. B. thanks the 5 × 1000 Anno 2020, Redditi 2019, ''Prevenzione, diagnosi e trattamento della fragilità ossea'' for funding this research.

References

1 H. Schultz, Sea Urchins: A Guide to Worldwide Shallow Water Species, 2006.
2 A. Miskelly, *Sea Urchins of the World: Diversity, Symmetry & Design*, Ashley Miskelly, 2009.
3 N. T. Shears and R. C. Babcock, *Oecologia*, 2002, **132**, 131.
4 N. Bianco-Stein, I. Polishchuk, A. Lang, L. Portal, C. Dejoie, A. Katsman and B. Pokroy, *Proc. Natl. Acad. Sci. U. S. A.*, 2022, **119**, e2120177119.
5 U. Magdans and H. Gies, *Eur. J. Mineral.*, 2004, **16**, 261.
6 I. Polishchuk, A. A. Bracha, L. Bloch, D. Levy, S. Kozachkevich, Y. Etinger-Geller, Y. Kauffmann, M. Burghammer, C. Giacobbe and J. Villanova, *Science*, 2017, **358**, 1294.
7 A. Berman, L. Addadi and S. Weiner, *Nature*, 1988, **331**, 546.
8 V. Presser, S. Schultheiß, C. Berthold and K. G. Nickel, *J. Bionic Eng.*, 2009, **6**, 203.
9 V. Presser, C. Kohler, Z. Živcová, C. Berthold, K. G. Nickel, S. Schultheiß, E. Gregorová and W. Pabst, *J. Bionic Eng.*, 2009, **6**, 357.
10 A. B. Smith, *Spec. Pap. Palaeontol*, 1980, **25**, 1.

11 H. Chen, T. Yang, Z. Wu, Z. Deng, Y. Zhu and L. Li, *Acta Biomater.*, 2020, **107**, 218.
12 M. Sancho-Tomas, S. Fermani, J. Gomez-Morales, G. Falini and J. M. Garcia-Ruiz, *Eur. J. Mineral.*, 2014, **26**(4), 523.
13 V. Presser, K. Gerlach, A. Vohrer, K. G. Nickel and W. F. Dreher, *J. Mater. Sci.*, 2010, **45**, 2408.
14 G. N. Jan and N. H. James, *Zoomorphology*, 2003, **132**, 301.
15 S. V. Dorozhkin, *Biomaterials*, 2010, **31**, 1465.
16 L. Cao, X. Li, X. Zhou, Y. Li, K. S. Vecchio, L. Yang, W. Cui, R. Yang, Y. Zhu and Z. Guo, *et al.*, *ACS Appl. Mater. Interfaces*, 2017, **9**, 9862.
17 K. S. Vecchio, X. Zhang, J. B. Massie, M. Wang and C. W. Kim, *Acta Biomater.*, 2007, **3**, 785.
18 Z. Deng and L. Li, *ACS Biomater. Sci. Eng.*, 2021, **9**(7), 3900.
19 S. Gärtner, A. Graf, C. Triunfo, D. Laurenzi, S. M. Schupp, G. Maoloni, G. Falini and H. Cölfen, *Int. J. Mol. Sci.*, 2022, **23**, 1.
20 S.-H. Wu, C.-Y. Mou and H.-P. Lin, *Chem. Soc. Rev.*, 2013, **42**, 3862.
21 S.-H. Wu, Y. Hung and C.-Y. Mou, *Chem. Commun.*, 2011, **47**, 9972.
22 F. Salamanna, G. Tedesco, M. Sartori, C. Griffoni, P. Spinnato, P. Romeo, R. Ghermandi, M. Fini, G. Giavaresi and A. Gasbarrini, *Front. Endocrinol.*, 2024, **14**, 1245344.
23 J. N. Weber, *Am. J. Sci.*, 1969, **267**, 537.
24 J. N. Grossmann and J. H. Nebelsick, *Zoomorphology*, 2013, **132**, 301.
25 B. Pokroy, A. N. Fitch, F. Marin, M. Kapon, N. Adir and E. Zolotoyabko, *J. Struct. Biol.*, 2006, **155**, 96.
26 A. Nouroozi Masir, A. Darvizeh and A. Zajkani, *J. Solid Mech.*, 2019, **11**, 902.
27 E. M. Gerhard, W. Wang, C. Li, J. Guo, I. T. Ozbolat, K. M. Rahn, A. D. Armstrong, J. Xia, G. Qian and J. Yang, *Acta Biomater.*, 2017, **54**, 21.
28 G. Magnabosco, I. Papiano, M. Aizenberg, J. Aizenberg and G. Falini, *Chem. Commun.*, 2020, **56**, 3389.
29 Y. Oaki, M. Kijima and H. Imai, *J. Am. Chem. Soc.*, 2011, **133**, 8594.
30 A. Dery, V. Guibourt, A. I. Catarino, P. Compère and P. Dubois, *Invertebr. Biol.*, 2014, **133**, 188.
31 E. Zolotoyabko and B. Pokroy, *CrystEngComm*, 2007, **9**, 1156.
32 B. Pokroy, J. P. Quintana, E. N. Caspi, A. Berner and E. Zolotoyabko, *Nat. Mater.*, 2004, **3**, 900.
33 M. Albéric, E. N. Caspi, M. Bennet, W. Ajili, N. Nassif, T. Azaïs, A. Berner, P. Fratzl, E. Zolotoyabko and L. Bertinetti, *et al.*, *Cryst. Growth Des.*, 2018, **18**, 2189.
34 C. Lauer, S. Haußmann, P. Schmidt, C. Fischer, D. Rapp, C. Berthold and K. G. Nickel, *Adv. Eng. Mater.*, 2020, **22**, 1900922.
35 Y. P. Guo and Y. Zhou, *Mater. Chem. Phys.*, 2007, **106**, 88.
36 R. Fernández-Penas, C. Verdugo-Escamilla, C. Triunfo, S. Gärtner, A. D'Urso, F. Oltolina, A. Follenzi, G. Maoloni, H. Cölfen and G. Falini, *J. Mater. Chem. B*, 2023, **11**, 7766.
37 A. Sibiya, J. Jeyavani, J. Sivakamavalli, C. Ravi, M. Divya and B. Vaseeharan, *Reg. Stud. Mar. Sci*, 2021, **44**, 101760.
38 L. Stabili, M. I. Acquaviva, R. A. Cavallo, C. Gerardi, M. Narracci and P. Pagliara, *J. Evidence-Based Complementary Altern. Med.*, 2018, 7891748.
39 Z. Chi, R. Liu, H. You, S. Ma, H. Cui and Q. Zhang, *PLoS One*, 2014, **9**, e102334.

